ECTI Transactions on Computer and Information Technology
Journal homepage: https://ph01.tci-thaijo.org/index.php/ecticit/
Published by the ECTI Association, Thailand, ISSN: 2286-9131

Edge-Morphology Detection Approach for Median Nerve Segmentation on Ultrasound Images

Kuenzang Thinley[1], Settha Tangkawanit[2] and Surachet Kanprachar[3]

ABSTRACT

Carpal Tunnel Syndrome (CST) is a form of peripheral neuropathy that affects a significant number of people. It is triggered by the compression of the median nerve in the wrist. CTS has recently been diagnosed using ultrasonography. This article presents a method that employs an edge-morphology detection approach to extract the structural feature of the median nerve from ultrasound images to permit automated segmentation of the median nerve. Pre-processing is applied to reduce the associated noise to boost the sensitivity and increase the accuracy of the model in segmenting the median nerve in ultrasound images. When tried on the test images, the suggested model performed well, with average precision, recall, F-score, and Jaccard similarity values of 0.87, 0.93, 0.76, and 0.93, respectively. Furthermore, a strong correlation of Cross-Sectional Area (CSA) between the ground truth and the segmented image of 0.962 is observed, allowing this model to serve as a useful initial screening tool to expedite the detection, diagnosis, and assessment of CTS in clinical practice.

Article information:

Keywords: Ultrasound image, Median nerve, Carpal Tunnel Syndrome (CTS), Signal processing, Segmentation, Edge-Morphology Detection

Article history:
Received: March 8, 2022
Revised: April 9, 2022
Accepted: April 23, 2022
Published: June 4, 2022 (Online)

DOI: 10.37936/ecti-cit.2022161.247832

1. INTRODUCTION

Carpal tunnel syndrome (CTS) is the most common kind of peripheral compression neuropathy, defined by entrapment of the median nerve at the wrist, resulting in median nerve dysfunction [1, 2]. The most important local symptoms CTS are that it increases the stiffness of the flexor retinaculum, causes inflammation of the flexor tendon sheath and anatomical variants of the nerve, especially with concomitant additional arteries and in the presence of anomalous muscles. Furthermore, systemic morbidities including obesity, diabetes, hypothyroidism, arthritis, or even physiological circumstances like menopause or pregnancy are established risk factors for CTS [3, 4].

The CTS condition affects 99 out of every 100,000 persons in the general population. Globally the prevalence rates range from 7% to 19% [5]. Although CTS is common to all age groups, people older than 40 are the most common age group who are likely to suffer from CTS and women account for about 65-75% of cases [6]. This is because women's carpal tunnels are smaller in comparison to those of a man. Women are also 3 to 5 times more likely than men to get Rheumatoid Arthritis, because many women go through pregnancy [7]. It affects the working population, with a focus on manual labour, but it also affects occupations that need sophisticated hand movements, such as musicians and dentists [8].

Lately, high-frequency ultrasound (US) imaging has been extensively adopted in various medical fields for the early diagnosis of the internal health of the human body. One such application is for tissue characterization, such as the assessment of musculoskeletal and neuromuscular diseases [9, 10], as well as peripheral nerve pathologies [11]. It has gained popularity because can present the nerve morphology. The results of many CTS patients were used to compare and verify the morphology of the median nerve using ultrasonography with other Nerve Condition Studies (NCSs) and clinical evaluation in [12, 13]. Ultrasound imaging has a sensitivity and specificity of up to 94% and 98%, respectively [14]. Despite numerous good results in earlier attempts to characterize, segment, and detect median nerves from US-based imaging, one drawback of US nerve imaging techniques is that it has significant variability, both across patients and in scanning parameters [15]. Tracking median nerve areas of interest with ultrasonic imaging is difficult [1] and challenging as it requires a very

[1,2,3]The authors are with Department of Electrical and Computer Engineering, Naresuan University, Phitsanulok, Thailand, E-mail: kuenzangt63@nu.ac.th, setthat@nu.ac.th and surachetka@nu.ac.th

experienced and skilled operator to detect the CTS from the US images. [16] investigated the segmentation of median nerves using the Greedy Active Contour detection (GACD) method. The reference contour remains a factor in contour computation. Contour segmentation may produce an incorrect result due to a defective contour in the reference image. Thus, understanding the deviation and displacement of the median nerve during diverse hand movements is therefore highly reliant on nerve segmentation and localization from the US images. To overcome such challenges, pre-processing and signal processing techniques should be applied. In this study, to get a better result compared to [16], additional signal processing feature extraction processing such as mathematical morphology operations and edge detection on top of contour features is adopted. Additionally, pre-processing for segmentation and detection of the median nerve is applied to aid in the automated extraction of shape attributes for the median nerve.

The following is a breakdown of how this article is structured. Section 2 of the article discusses the related theory pertaining to the study. Section 3 presents how data was collected and the overall methodology adopted to segment the median nerve in ultrasound images. Furthermore, the influence of signal processing techniques in segmenting the median nerve in an ultrasound image is presented in Section 4, which contains the experimental results and a discussion on test ultrasound image datasets. Finally, the conclusion in Section 5 presents the summary of the performance of the model on the test data and its assistance in the initial screening tool to expedite the detection, diagnosis, and assessment of CTS in clinical practice and also discusses some of the limitations.

2. RELATED THEORY

2.1 Image Denoising

Speckle noise is the predominant multiplicative noise that deteriorates the quality of ultrasound images [17]. The constructive and destructive coherent interference of backscattered echoes from scatterers that are often considerably smaller than the spatial resolution of medical ultrasonography systems create speckle in US B-scans, which appear as a granular texture [18]. Speckle lowers contrast and impairs target delectability in B-scan images, affecting a human's ability to distinguish between normal and diseased tissue. It also slows down and distorts ultrasonic image processing operations like segmentation and registration. Many methods have been proposed to despeckle the noise [19]. Traditional filters such as lee, Kaun, frost, median, and hybrid filters, as well as wavelet filters, are used in the speckle noise reduction approaches.

The most difficult aspect of image denoising is preserving data with structures, such as edges and surfaces, to achieve rich visual quality while improving the Signal-to-Noise Ratio (SNR). Image denoising with edge protection in the medical image is crucial as edges define the important characteristics between normal features and abnormalities in medical images. This study used a bilateral filter [20] which is a non-linear image smoothing filter that preserves edges while lowering noise. It uses a weighted average of intensity data from surrounding pixels to replace the intensity of each pixel. The weights and radiometric discrepancies influence the pixel's Euclidean distance. Mathematically the bilateral filter is defined by (1).

$$BF[I]_p = \frac{1}{W_p}\sum_{x_i \in S} {}^{I(x_i)G_r(\|I(x_i)-I(x)\|)\cdot}_{G_s(x_i-x)} \tag{1}$$

W_p is a normalization factor that controls the smoothness of the image. W_p is defined by (2).

$$W_p = \sum_{x_i \in S} G_r(\|I(x_i - I(x)\|)G_s(x_i - x) \tag{2}$$

$BF[I]_p$ is the filtered image. $I(x_i)$ is the original ultrasound input image. x is the current pixel coordinate of the image to be filtered. S defines the window centered for x. G_s and G_r are the kernel range for smoothing images in intensities and spatial kernel for smoothing different coordinates, respectively.

The input median nerve ultrasound image used in this work was filtered using kernel values (S, G_s, G_r) $= (9, 18, 85)$ as the optimal values. A value of G_s and G_r lower than 18 has a small effect and values greater than 85 make the image too smooth and blurs some edges of the median nerve structure. Furthermore, a kernel value or window size S less than 9 makes little impact on noise removal.

Fig. 1 shows the comparison of different filters in removing the noise from an ultrasound image. There are 5 images including the original image, the threshold image, and the filtered images from 3 different types of filtering.

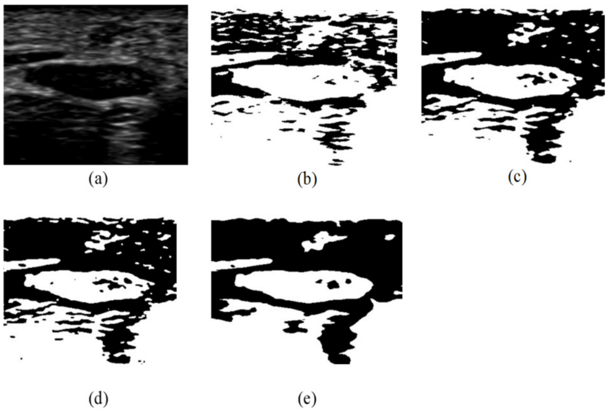

Fig.1: *Image Filtering (a) Original Image (b) Threshold Input Image (c) Gaussian Filter (d) Median Filter (e) Bilateral Filter.*

Fig.1(a) and (b) represent the original image and the corresponding threshold image. The threshold image (Fig. 1(b)) shows that along with the major median nerve structure, there are tiny segments of noise speckle that surround them, making the analysis difficult. To minimize noise, Gaussian (Fig.1(c)) and Median (Fig.1(d)) filters are used. Although these filters may reduce noise by a certain proportion, they also fade the median nerve's edges, which is crucial for analysis. In comparison to other filters such as the Gaussian filter (Fig.1(c)) and the Median filter (Fig.1(d)), the bilateral filter not only reduces noise but also keeps and preserves the fine borders of the median nerve structure (Fig.1(e)). This demonstrates the advantage of the bilateral filter in reducing speckle-noise while preserving fine edges as compared to the other filters (Gaussian and median).

2.2 Contrast Enhancement

Contrast enhancement is a crucial part of image processing for both human and machine vision. It is commonly used in medical image processing, as well as speech recognition, texture synthesis, and a variety of video processing applications as a pre-processing step. Due to the intrinsic properties of medical images, such as poor contrast, speckle noise, signal dropouts, and complicated anatomical structures, medical image analysis is a particularly tough challenge to solve. As a result, before further processing and analysis, it is critical to improve the contrast of such images. The primary reason for this is that if the input image is of poor quality and contrast, further processing processes such as image segmentation, feature extraction, and image classification will fail. The performance of pre-processing procedures such as image enhancement, for example, will have a direct influence on any subsequent processing. As a result, high-performance image-enhancing algorithms can improve total system performance dramatically. Histogram equalization (HE) is a frequently used technique for increasing visual contrast. Its core concept is to map gray levels using the probability distribution of the input gray levels. Suppose an input image $g(x, y)$ is composed of discrete gray levels in the dynamic range of $[0, L{-}1]$. The transformation mapping $C_{(rk)}$ of HE is given by (3).

$$s_k = C(r_k) = \sum_{i=0}^{k} P(r_i) = \sum_{i=0}^{k} \frac{n_i}{n} \tag{3}$$

$0 \leq s_k \leq 1$ and $k = 0, 1, 2, \ldots, L{-}1$. n_i represents the number of pixels having a gray level r_i. n is the total number of pixels in the input image. $P(r_i)$ represents the Probability Density Function (PDF) of the input gray level r_i. Based on the PDF, the Cumulative Density Function (CDF) is defined as $C(r_k)$. This mapping in (3) is called Global Histogram Equalization (GHE) or Histogram Linearization. This approach uses the image histogram to spread out the gray levels in a picture and reassigns the brightness value of pixels. The Global histogram equalization (GHE) approach works best when the original image has little contrast to begin with. Otherwise, histogram equalization may compromise image quality. If the image has certain gray levels with high frequencies, they can dominate the low-frequency gray levels. GHE remaps the gray levels in this situation so that contrast stretching is limited in some dominating gray levels with larger image histogram components, while significant contrast loss occurs in others. In other words,it yields either too dark or too bright regions in the image. The contrast limited adaptive histogram (CLAHE) method is another technique to enhance the contrast of the image which overcomes the disadvantage of GHE. It is a hybrid of HE and adaptive histogram equalization in which the histogram is adaptively equalized in blocks with a predetermined clip limit. CLAHE does not function on the entire image. Instead, it operates on tiny areas of the image known as tiles. It works the same way on each tile as regular Histogram Equalization (HE) [21, 22].

2.3 Mathematical Morphology

Mathematical morphology is a nonlinear image processing approach based on an object's geometric structure or form. It uses set theory to modify an image's geometric structure. It is widely used for noise reduction, feature extraction, edge detection, image segmentation, form identification, image comparison, and texture analysis [23]. The mathematical morphology algorithm is a representation of the interaction between a set of objects and their structural components. The structuring element which is also referred to as the kernel window plays an important part in the morphology operation. The structuring element is shifted across the length and width of the image to perform the morphology operation. Dilation, erosion, opening, and closure are the four main operations of mathematical morphology. They have distinct characteristics in binary and grayscale images. Based on these fundamental procedures, several useful mathematical morphology methods might be constructed and integrated for different applications. The basic operation of dilation and erosion is given by equations (4) and (5).

Dilation operation: dilation of binary image A by structuring element B $(A \oplus B)$ which is mathematically shown in (4).

$$A \oplus B = \bigcup_{b \in B} A_b \tag{4}$$

Erosion operation: erosion of binary image A by structuring element B $(A \ominus B)$ which is mathematically represented by (5).

$$A \ominus B = \bigcap_{b \in B} A_{-b} \tag{5}$$

Dilation is an expanding procedure that expands the target while contracting the hole, allowing the user to merge background points surrounding the image and link two neighbouring items. Erosion, on the other hand, is a contractive process that causes the target to contract and the hole to enlarge to remove unnecessary points and separate two small, related objects.

3. METHODOLOGY

This section discusses the segmentation framework to detect the median nerve from the ultrasound images using the signal processing techniques framework. Fig.2 shows the overall methodology adapted for the study.

Overall, there are two stages involved in the segmentation of the median nerve on ultrasound images: namely the pre-processing, and the signal processing stages. The pre-processing stage includes the ROI selection, image denoising, image contrast enhancement, and thresholding. The signal processing stage extracts the feature of the input image. The techniques used in this stage are edge detection, morphology operation, and contouring.

3.1 Data Collection

As shown in Fig.2, the input images are from the ultrasound images obtained as secondary data from a hospital in Phitsanulok province, Thailand. In the data collecting procedure, however, no physical experiment of the patient or individual was involved. The ultrasound images of wrists that had already been experimented with in previous years and stored in the ultrasound machine's database were collected for study purposes. The experiments were carryout by a trained specialist (a medical doctor). The examination was examined using SONIMAGE HS1, Konica Minolta, a portable ultrasound machine. In total,

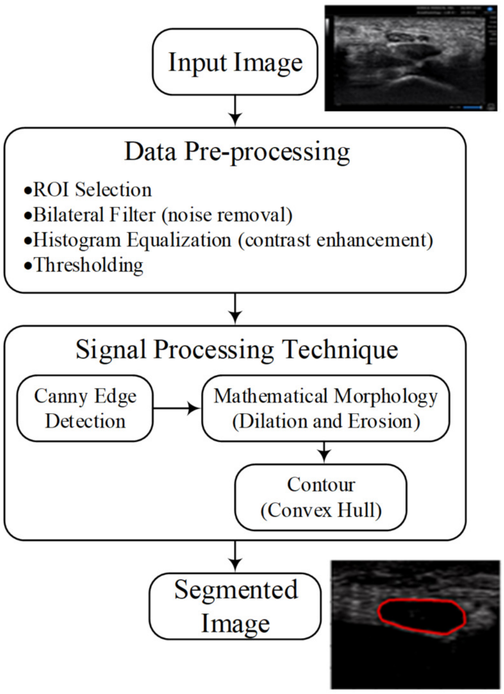

Fig.2: *Architecture of Median Nerve Segmentation using Signal Processing Algorithm.*

35 ultrasound hand wrist images of distal type were collected. The size of each image is 864×648 pixels.

3.2 Pre-processing and Segmentation Phase

To illustrate in detail of the pre-processing and signal processing shown in Fig.2, the flow chart of these two stages is given in Fig.3. For the pre-processing stage, the input image in gray scale is fed to the system. Such an image is filtered by a bilateral filter using (1) and (2). The input image ROI is then selected. The image contrast is modified using CLAHE by (3). At the end of this satge, the image is changed from a gray-scale image to a binary image using Otsu. The result from applying these pre-processing techniques is given next.

Pre-processing is applied to minimize the complexity, to improve the accuracy of the applied algorithm, and remove the noise. It also increases the sensitivity of segmenting the median nerve in ultrasound images. The pre-processing techniques adopted in this study are image denoising, ROI selection, contrast enhancement, and thresholding. An input gray-scale image with a size of 864×648 pixels is first passed through a bilateral filter to smooth the image. Such filtering preserves edges while lowering noise and is applied to minimize the speckle noise which is the predominant multiplicative noise in ultrasound images.

A square ROI with a size of 432×432 pixels from the canter of the 864×648 pixels in the original image is selected. The center of the image is the most credible and provides an optimal spot to avoid any distorting effects in ultrasound wave patterns as shown

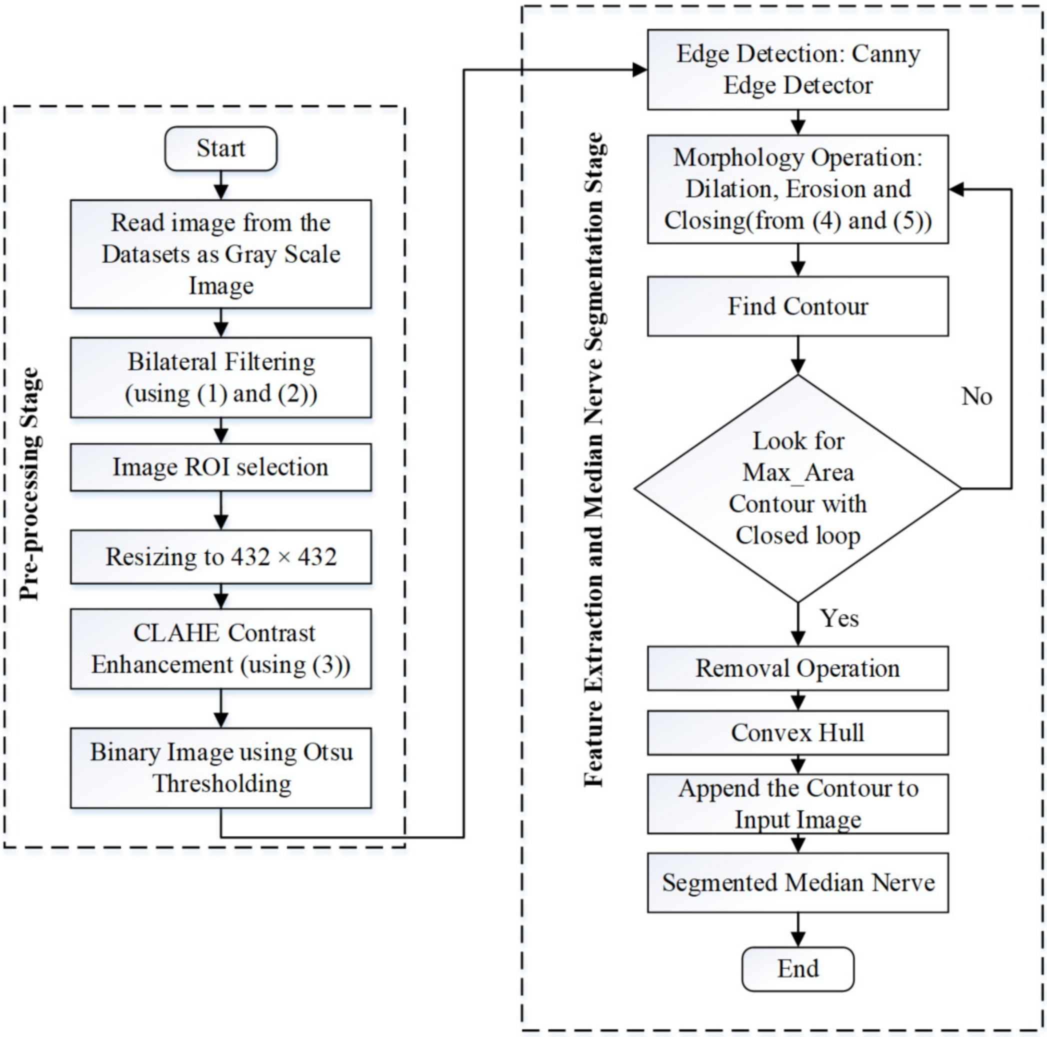

Fig.3: *Flow Chart of the Proposed Method.*

in Fig.4. Furthermore, using an ROI to extract features from a subset of an image rather than the entire image minimizes the computing time.

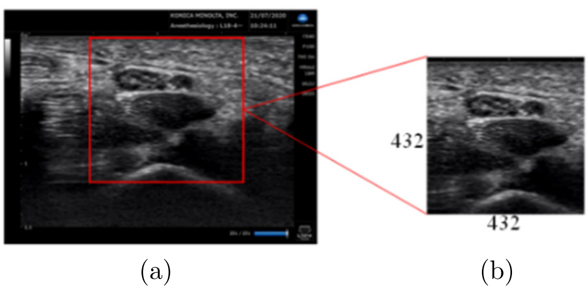

Fig.4: *ROI Selection.*

From Fig.4(a), it can be seen that from the original input image with a size of 864×648 pixels, there is an area where most of the pixels are in black (lower portion of the image) while in some area the values of the pixels seems to be randomly combined pixels ranging between black and white (upper portion of the image). From an Information Theory point of view, the upper portion of the image contains more information than the lower portion. Thus, in the ROI selection process, the upper part of the image should be selected. This is shown in Fig.4(b). Thus, using an ROI to extract features from a subset of an image rather than the entire image will lower the computing time and power required.

The contrast limited adaptive histogram (CLAHE) method is then applied to enhance the contrast of the image. CLAHE remaps the contrast of the image adaptively because the histogram is adaptively equalized in blocks with a predetermined clip limit. CLAHE does not function on the entire image. Instead, it operates on tiny areas of the image known as tiles. Fig.5 shows the effects of GHE and CLAHE on image enhancement.

Fig.5(b) shows that the GHE equalization stretches the contrast of an image so regions of it are either too dark or too bright. Fig.5(c) depicts the effects of CLAHE equalization in which the contrast of the image is stretched adaptively. Fig.6 shows the histogram of the original and the CLAHE equalized

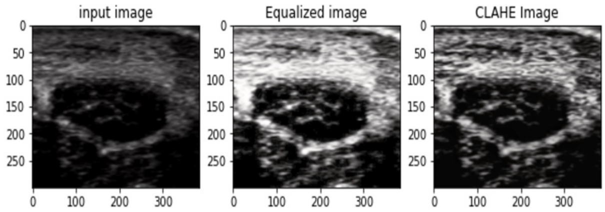

(a) (b) (c)

Fig.5: *(a) Original Image (b) Global Histogram Equalization (c) Adaptive or Local Histogram Equalization.*

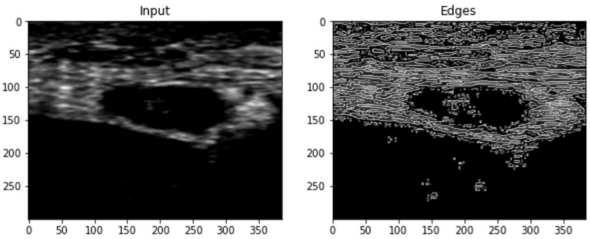

(a) (b)

Fig.7: *Effect of Edge Detection: (a) Input Image and (b) Edge-Detected Image.*

image. As shown in the diagram, the histogram of the original image (Fig.6(a)) is more skewed towards 0 to 155 compared to the CLAHE equalized image (Fig.6(b)) whose histogram intensity is almost uniformly distributed across 0 to 255. After CLAHE, the image can be binarized using Otsu thresholding [24].

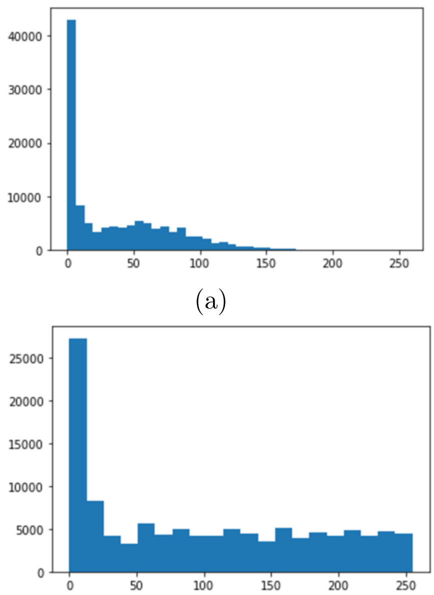

(a)

(b)

Fig.6: *(a) Histogram of Original Image (b) Histogram of CLAHE Equalized Image.*

For the signal processing stage, the canny operator is used as the edge detection method to determine the structure of the median nerve in an ultrasound image to divide the region. This well-known edge identification approach helps to simplify image analysis by dramatically lowering the quantity of data that must be processed while keeping important structural information about median nerve borders.

The output of binary images from the edge detection procedure appeared to cause a serious difficulty when the system was initially run. Unexpectedly, as shown in Fig.6, the edge detected output contains several edge lines that do not represent the median nerve.

Because there are so many edges along with the genuine median nerve edges, as seen in Fig.7(b), it would be extremely difficult to produce the true median nerve shape. The issue arose because the canny edge detector was unable to filter the image's minor marginal differences in gray color, making it impossible to determine the canny edge detector's upper and lower threshold values. It takes longer to choose the threshold value using the trial-and-error technique.

To solve this problem, the Euler number approach [25] was used before the edge identification procedure. The Euler number is utilized to extract the median nerve area in an ultrasound image with this procedure. The strategy relies on the ultrasound image's connectedness and holes. The Euler number, E, is the basic relationship between the number of linked object components, C, and the number of holes (H) in an image given by (6).

$$E = C - H \tag{6}$$

The Euler number approach is used to link the pixels in the median nerve region, isolating them from the undesirable surrounding area known as the object holes. Edge detection after applying the Euler number approach is shown in Fig.8. When compared to the result of Canny edge detection, it demonstrates that the edges are more meaningful with definite distinction between the median nerve structure and other non-media structure components. It can be used to distinctly distinguish the median nerve.

Once the edge has been detected, a mathematical morphological method called dilation is used to extend the edge such that it encompasses the anatomical region of interest. To ensure that the growth process does not continue beyond the interest region, an appropriate dilation value is computed by repetitive iteration. Any undesired growth regions will be removed as a precautionary approach.

As a result, dilation reunites the disjointed dotted edge lines, particularly those that make up the median area shape. The erosion then eliminates the unnecessary edge line that connects the specified region. After the median nerve region's edge has been produced as a closed rounded line, the close operation is performed to close the rounded boundary. The region

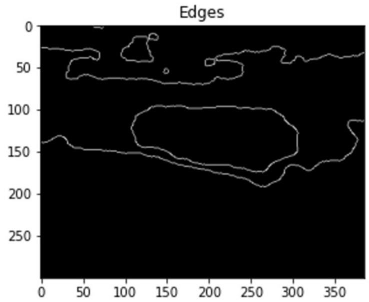

Fig.8: *Edge Detection after Applying for Euler Number Approach.*

area is filled to create a region of interest (ROI). The ROI is significant since it will be used as the image mask for another detection task shortly after. The removal operation is performed to separate each ROI from its adjacent region, which may contain other undesirable areas, particularly those tiny portions next to the median nerve area. The result is a single object (As shown in Fig.9). A convex hull is used to define the contour to join some small disjoint parts in the segmented median nerve boundaries.

3.3 Evaluation Matrix

Evaluation indices such as the Jaccard similarity coefficient (JC), recall (R), precision (P), and $F1$ score are used as the performance evaluation metrics in the median nerve segmentation task. They are evaluated by comparing the ground truths to the automated segmentation outputs using the spatial overlap percentage between two binary images as a metric. The score might range from 0 to 1, with 0 indicating no overlap and 1 indicating a perfect match. Mathematically, these indices can be represented by the equations (7) to (10).

$$JC = \frac{|A \cap B|}{|A \cup B|} \tag{7}$$

$$R = \frac{TP}{TP + FP} \tag{8}$$

$$P = \frac{TP}{TP + FP} \tag{9}$$

$$F1 \text{ Score } = 2 \times \frac{R \times P}{R + P} \tag{10}$$

The TP, TN, FP, and FN represent the pixel numbers of true positive, true negative, false positive, and false negative, respectively. A represents the ground truth of the median nerve annotated manually by the sonographer. B denotes the predicted or automatically segmented median nerve region by the proposed algorithm. Furthermore, the cross-sectional area (CSA) of the segmented median nerve is calculated to check the presence of CTS.

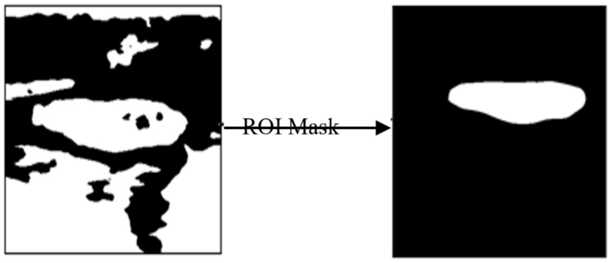

Fig.9: *ROI Mask after Morphology Operation.*

4. EXPERIMENT RESULTS AND DISCUSSION

4.1 Experiment Setup

The experimental setup is presented in Table 1 with values. The test images were obtained from the hospital as secondary images. The segmentation of the median nerve was implemented using the OpenCV image processing library and the open source python language. Each of the 35 test images has a varied image quality and contrast, and has a different structure or form of the median nerve. Fig. 10 shows a sample test image. Figures in Fig.10(a) depict a condition in which the input ultrasound image cannot distinguish between the median nerve structure and its surroundings, and no identifiable border between the median nerve structure and its surroundings can be seen.

Table 1: *Experimental Setup Environment.*

System	Name	Specifications/version
Hardware	Personal Laptop	Lenovo, 16GB RAM, Intel Core i7-9750H CPU @ 2.60GHz - 5.00GHz, GPU @ NVIDIA Quadro T2000
Programming Language	Python	3.7
Editor	VS Code	1.58
Test Image	Ultrasound image	35 test images with a size of 864 × 648 pixels
Library	Open CV	4.5.4

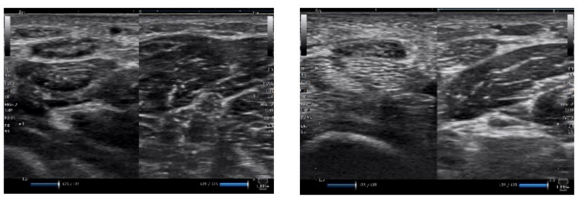

(a) (b)

Fig.10: *Sample of Test Image.*

4.2 Experiment Result

A qualitative evaluation was performed by visually inspecting how well the segmented results were fitted to the true boundary of the median nerve. Fig.11 compares the manually segmented median done by experts with the median nerve segmented by the proposed study.

Fig.11(a) shows the initial wrist ultrasound scan, which shows the median nerve's structural information. Fig.11(b) shows the image segmented manually by an experienced sonographer, whereas (Fig.11(c)) which is contoured with red contour shows the image segmented using the proposed edge-morphology (signal processing) approach. In comparison to the manually segmented picture (Fig. 11(b)), the suggested method's segmented output (Fig. 11(c)) shows that the generated median nerve contours overlaid onto the genuine border of the median nerve. It can be seen in (Fig.11(b)) that a section of the real median nerve border is left unsegmented, as indicated by the little red rectangle. As can be seen, the suggested segmented image shows a superior level of precision and accuracy in the median nerve segmentation.

In addition to the qualitative evaluation, the accuracy of the model was further confirmed by comparing the automatic findings to the ground truth which was manually segmented by the sonographer. Indices shown by (7) to (10) were used to measure the performance of the proposed method.

The algorithm was tested on 35 ultrasound images and obtained precision, recall, F1-score, and Jaccard similarity of 0.87,0.93, 0.76, and 0.93 respectively, which shows that there is a higher degree of overlap between the segmented and ground truth image. The ground truth is achieved by conducting manual area tracing on the median nerve using GIMP 2.10.28 (GNU Image Manipulation Program), a free and open-source raster graphic tool, on the manually marked ultrasound image by the expert sonographer. When the tracing was completed, the selected region was highlighted and changed to a binary image (foreground as white and background as black).

Fig.12(a) to 12(f) illustrate some of the median nerve segmentation findings utilizing the suggested technique. The image without a contour is the test image or input image, while the image marked with a red contour is the corresponding segmented image from the proposed method. The real boundary of the median nerve is precisely segmented, as can be seen in the result images.

Fig.12(a) and 12(b) represent the segmentation result when the input image is highly clean, with a defined border between the actual median nerve structure and the surroundings. The segmented images can be easily obtained. Fig.12(c) and 12(d) represent the segmentation result from the second scenario when the contrast of an input image is not equally distributed and the true border between the genuine median nerve is noisy. With the proposed method, the input images can also be segmented. Fig.12(e) and 12(f) show the segmentation result from the proposed system in the worst-case situation when the input ultrasound image cannot discriminate between the median nerve structure and its surroundings, and there is no discernible border between the structure of the median nerve and its surroundings. Interestingly, the proposed method can do the segmentation work, as well. The resilience and the robustness of the suggested model in segmenting the median nerve efficiently in ultrasound images despite higher variability in the input image is demonstrated by these different case outcomes.

4.3 Discussion

With no manual intervention, the edge-morphology approach was able to properly localize and segment the median nerve. The cross-sectional area (CSA) of the segmented median nerve was calculated and compared to the CSA of ground truth (GT) to ascertain the effectiveness of the algorithm. The cross-sectional area (CSA) of the median nerve (MN) is the most often used parameter to measure and quantify the CTS, with cut-off values diagnostic for MN pathology defined from 9 mm^2 to 14 mm^2 in various analytical settings [19]. However, the value of 9 mm^2 for the median nerve area is the most trusted cut-off value for MN pathology during CTS as shown by NCSs investigations.

Fig.13 compares the cross-sectional area (CSA) of the median nerve between the original image or ground truth (GT) and the segmented median nerve from the proposed algorithm. The green dashed line represents the CSA value calculated by the expert and the blue solid line illustrates the CSA value of the median nerve calculated using the proposed algorithm. It is evident from the figure that there is a significant correlation of CSA between the original image and the segmented image with a close resemblance of over 90%. This promising result proves that the proposed algorithm can be used in clinical practice to aid in diagnosing CTS in ultrasound images. The average and standard deviation from these two cases are determined and shown in Table 2.

Table 2 shows the average CSA value of ground truth and the mean value determined using the proposed method. The ground truth and proposed methods yielded average CSA values of 12.8 $mm^2 \pm 4.384$ mm^2 and 11.95 $mm^2 \pm 3.909$ mm^2, respectively. The table shows that the average CSA value acquired using the proposed method is nearly identical to the value determined by the professional sonographer. Furthermore, the standard deviation determined from the proposed method is also equivalent to the ground truth. This demonstrates that the model performs in the same way as the ground truth. It indicates that the proposed approach is uniform and

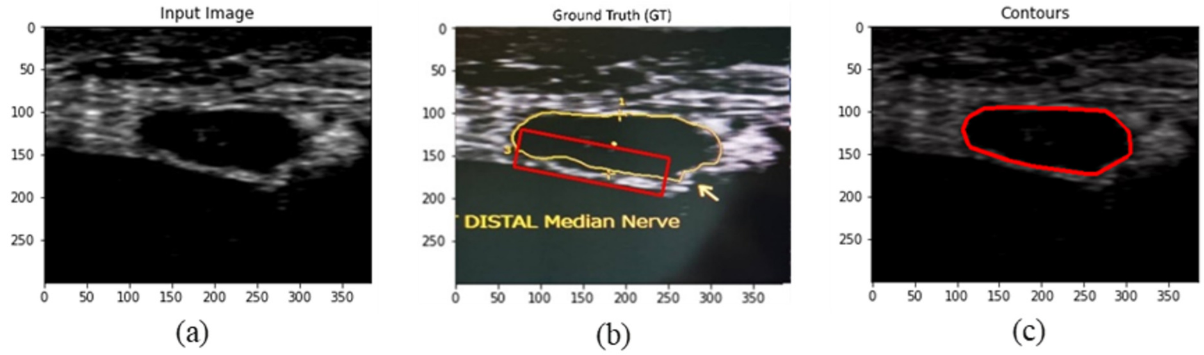

Fig.11: *Median Nerve Segmented (a) Original Input Image, (b) Ground Truth (GT) Segmented by A Sonographer, and (c) Automatic Median Nerve Segmented by the Proposed Algorithm.*

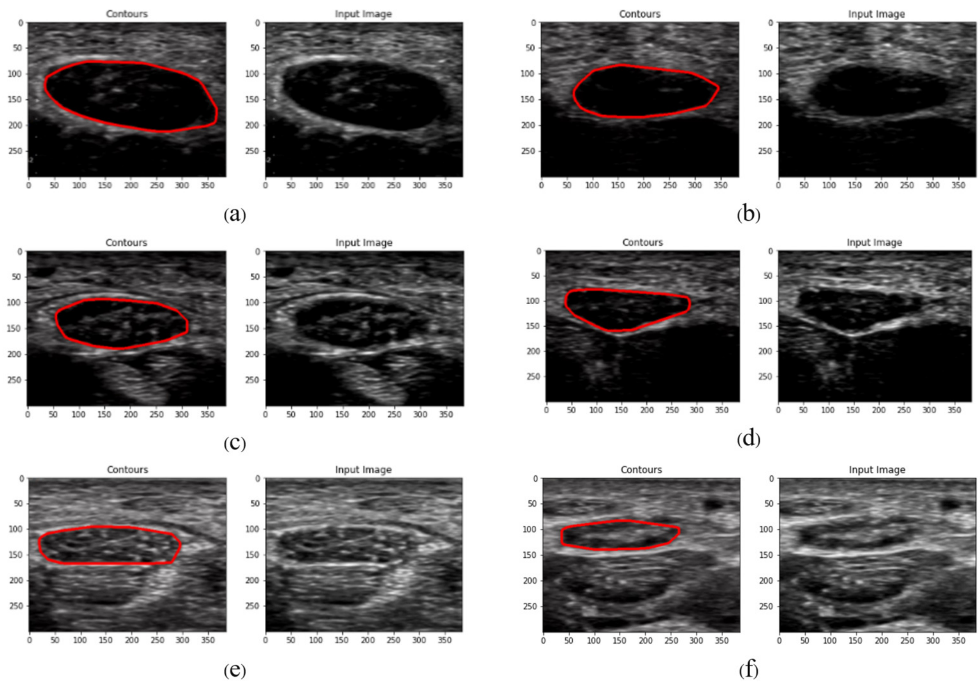

Fig.12: *Segmentation Result of Median Nerve Ultrasound Images using Proposed Method. The images with red contour shows the automatically segmented image using the proposed method and the images without contour are the test images.*

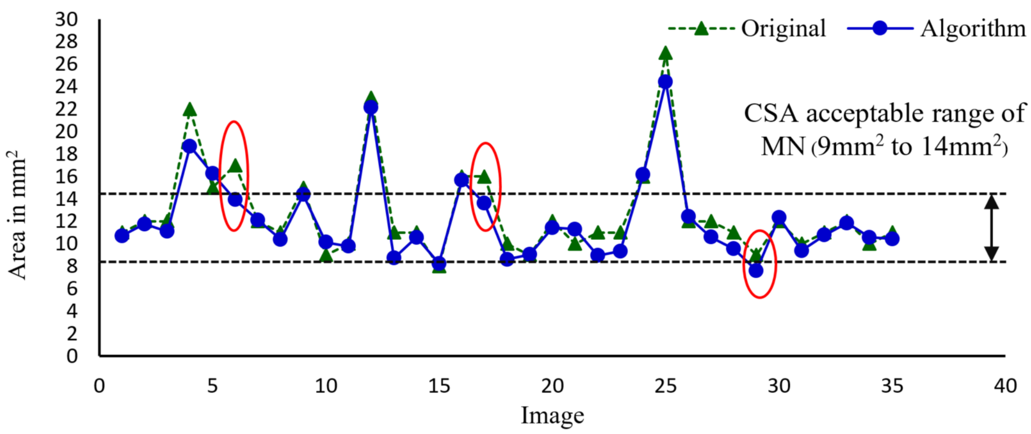

Fig.13: *Comparison of MN Cross-Sectional Area (CSA) between the Original Image and the Proposed Algorithm.*

resilient in the segmentation of the median nerve. It also concludes that the proposed model is stable and effective. As a result, it can be concluded that suitable data pre-processing introduced before the feature extraction model produces a high accurate result in the segmentation of median nerve in ultrasound images. Additionally, it does not demand the sonographer to manually detect and identify the median nerve to diagnose carpal tunnel syndrome (CTS), which requires a lot of experience and time. As a result, the proposed approach can be employed to segment the median nerve in an ultrasound machine to diagnose CTS.

Table 2: *The Mean and Standard Deviation of Cross-Sectional Area (CSA) Value from Original Image (or Ground Truth) and Proposed Algorithm.*

Model	CSA (Mean ± SD) in mm^2
Original Image (Ground Truth)	12.8 ± 4.384
Proposed Algorithm	11.95 ± 3.909

However, the model has estimated the CSA of the median nerve as false positive (represented by the red circle marked in Fig.13) in some situations, even when the expert or sonographer evaluated it as true positive. Image numbers 6 and 17 in Fig.13 are classed as normal (i.e., the 13.9 mm2 and 13.8 mm2 are CSA of the segmented image, and 17.32 mm2 and 16 mm2 are the CSA calculated by the expert sonographer, respectively). Additionally, for image number 29, from the proposed algorithm, it has been determined as abnormal with the CSA value of 9.2 mm2 while this has been assigned as a normal case by the expert. This may be the outcome of excessive erosion and dilatation during the morphological procedure. These issues could be further analyzed and might be solved by using more precise techniques like artificial intelligence and deep learning.

To show the degree of similarities in greater detail, statistical analysis is performed using Microsoft Excel (Microsoft 365). The correlation coefficient (also known as Pearson's product-moment "r") is used to determine the strength of the CSA's linear relationship with the ground truth and segmented image. In the examination of 35 test images, the CSA values from ground truth and the segmented image had a correlation coefficient of 0.962. These results suggest that the two CSAs (calculated and ground truth) have a strong association and again confirm that the proposed algorithm is a promising method for segmenting the median nerve.

To further present the usefulness of the proposed algorithm, some key performance indicators obtained from the proposed algorithm and work done previously are compared as shown in Table 3.

Table 3: *Comparison of Proposed Algorithm with other Method based on Signal Processing Algorithm.*

Model	Precision (%)	Recall (%)	F-1 Score (%)	Jaccard Similarity (%)
Wang's work [16]	85	91	75	-
Proposed Algorithm	87	93	76	93

Table 3 shows the comparison of the proposed algorithm with the work done by Wang [16] based on the signal processing techniques to detect the median nerve in ultrasound images. In Wang's work [16], a greedy active contour-based detection framework was used to detect the median nerve in ultrasound images. When tested on the test image, it obtained mean precision, recall, and F-1 score values of 85%, 91%, and 75%, respectively. The reference contour remains a factor in contour computation. Contour segmentation may produce an incorrect result due to a defective contour in the reference image. The proposed algorithm obtained mean precision, recall, and F-1 score values of 87%, 93%, and 76%, respectively. These are 2%, 2%, and 1% higher than [16]. Note that there is no information about Jaccard Similarity provided by [16]. The obtained improvement is from the pre-processing and additional signal processing techniques used in the proposed algorithm. This demonstrates that the proposed method is more dependable and consistent in median nerve segmentation.

5. CONCLUSION

This study found that signal processing techniques can be used to segment the median nerve in ultrasound images to calculate the characteristics of the median nerve. Data pre-processing aids the segmentation process by removing unwanted noise which adds complication to detecting the median nerve. Applying the proposed signal processing method, the median nerve can be segmented, and the cross-sectional area can be determined. It has been shown that the segmented area and the cross-sectional area of the proposed method are almost identical to those done by professional sonographers. In practice, the methodology can help establish a reliable technique to diagnose CTS in ultrasound images. This approach will also assist in the prediction of CTS treatment results. It will also lessen reliance on an experienced sonographer to recognize the median nerve in an ultrasound image, allowing it to be used as a predictive model notifying both the physician and the patient about the likelihood of success, easing their collaborative decision-making process.

ACKNOWLEDGEMENT

This study was supported by the Faculty of Engineering, Naresuan University, Phitsanulok, Thailand. Also, we would like to thank Fort Somdej Phra Naresuan Maharaj Hospital, Phitsanulok, Thailand for providing the data of ultrasound images for the study.

References

[1] M.-H. Horng, C.-W. Yang, Y.-N. Sun, and T.-H. Yang, "Deepnerve: A new convolutional neural network for the localization and segmentation of the median nerve in ultrasound image sequences," Ultrasound in Medicine & Biology, vol. 46, no. 9, pp. 2439-2452, 2020, doi: https://doi.org/10.1016/j.ultrasmedbio.2020.03.017.

[2] J. Wipperman and K. Goerl, "Carpal tunnel syndrome: diagnosis and management," *American Family Physician*, vol. 94, no. 12, pp. 993-999, 2016.

[3] J.-J. Park, J.-G. Choi, and B.-C. Son, "Carpal tunnel syndrome caused by bifid median nerve in association with anomalous course of the flexor digitorum superficialis muscle at the wrist," *The Nerve*, vol. 3, no. 1, pp. 21-23, 2017.

[4] L. Padua et al., "Carpal tunnel syndrome: clinical features, diagnosis, and management," *The Lancet Neurology*, vol. 15, no. 12, pp. 1273-1284, 2016.

[5] L. Newington, E. C. Harris, and K. Walker-Bone, "Carpal tunnel syndrome and work," *Best Practice & Research Clinical Rheumatology*, vol. 29, no. 3, pp. 440-453, 2015.

[6] S. F. Duncan and R. Kakinoki, "Carpal Tunnel Syndrome and Related Median Neuropathies," *Carpal Tunnel Syndrome and Related Median Neuropathies*, 2017.

[7] V. Kazantzidou, D. Lytras, A. Kottaras, P. Iakovidis, I. Kottaras, and I. P. Chatziprodromidou, "The efficacy of manual techniques in the treatment of carpal tunnel syndrome symptoms: A narrative review," *Int. J Orthop Sci*, vol. 7, no. 2, pp. 423-427, 2021.

[8] C. L. Burton, Y. Chen, L. S. Chesterton, and D. A. van der Windt, "Trends in the prevalence, incidence and surgical management of carpal tunnel syndrome between 1993 and 2013: an observational analysis of UK primary care records," *BMJ open*, vol. 8, no. 6, p. e020166, 2018.

[9] K.-V. Chang, W.-T. Wu, D.-S. Han, and L. Özçakar, "Static and dynamic shoulder imaging to predict initial effectiveness and recurrence after ultrasound-guided subacromial corticosteroid injections," *Archives of Physical Medicine and Rehabilitation*, vol. 98, no. 10, pp. 1984-1994, 2017.

[10] K.-V. Chang, W.-T. Wu, K.-C. Huang, W. H. Jan, and D.-S. Han, "Limb muscle quality and quantity in elderly adults with dynapenia but not sarcopenia: an ultrasound imaging study," *Experimental Gerontology*, vol. 108, pp. 54-61, 2018.

[11] J. Im Suk, F. O. Walker, and M. S. Cartwright, "Ultrasonography of peripheral nerves," *Current Neurology and Neuroscience Reports*, vol. 13, no. 2, p. 328, 2013.

[12] P.-H. Su, W.-S. Chen, T.-G. Wang, and H.-W. Liang, "Correlation between subclinical median neuropathy and the cross-sectional area of the median nerve at the wrist," *Ultrasound in Medicine & Biology*, vol. 39, no. 6, pp. 975-980, 2013.

[13] J. Y. Al-Hashel et al., "Sonography in carpal tunnel syndrome with normal nerve conduction studies," *Muscle & Nerve*, vol. 51, no. 4, pp. 592-597, 2015.

[14] I. Duncan, P. Sullivan, and F. Lomas, "Sonography in the diagnosis of carpal tunnel syndrome," *AJR. American Journal of Roentgenology*, vol. 173, no. 3, pp. 681-684, 1999.

[15] M. Byra, E. Hentzen, J. Du, M. Andre, E. Y. Chang, and S. Shah, "Assessing the performance of morphologic and echogenic features in median nerve ultrasound for carpal tunnel syndrome diagnosis," *Journal of Ultrasound in Medicine*, vol. 39, no. 6, pp. 1165-1174, 2020.

[16] Y.-W. Wang, C.-J. Chen, S.-F. Huang, and Y.-S. Horng, "Segmentation of Median Nerve by Greedy Active Contour Detection Framework on Strain Ultrasound Images," *J. Inf. Hiding Multim. Signal Process.*, vol. 6, no. 2, pp. 371-378, 2015.

[17] O. V. Michailovich and A. Tannenbaum, "Despeckling of medical ultrasound images," *IEEE Transactions on Ultrasonics, Ferroelectrics, and Frequency Control*, vol. 53, no. 1, pp. 64-78, 2006.

[18] S. K. Narayanan and R. Wahidabanu, "A view on despeckling in ultrasound imaging," *International Journal of Signal Processing, Image Processing and Pattern Recognition*, vol. 2, no. 3, pp. 85-98, 2009.

[19] A. Torres-Costoso, V. Martínez-Vizcaíno, C. Álvarez-Bueno, A. Ferri-Morales, and I. Cavero-Redondo, "Accuracy of ultrasonography for the diagnosis of carpal tunnel syndrome: a systematic review and meta-analysis," *Archives of Physical Medicine and Rehabilitation*, vol. 99, no. 4, pp. 758-765. e10, 2018.

[20] C. Tomasi and R. Manduchi, "Bilateral filtering for gray and color images," in *Sixth International Conference on Computer Vision (IEEE Cat. No. 98CH36271)*, 1998: IEEE, pp. 839-846.

[21] H. S. Ahmed and M. J. Nordin, "Improving diagnostic viewing of medical images using enhancement algorithms," *Journal of Computer Science*, vol. 7, no. 12, p. 1831, 2011.

[22] Z. M. A. Faten A. Dawood, "The Importance of

Contrast Enhancement in Medical Images Analysis and Diagnosis," *International Journal of Engineering Research & Technology (IJERT)*, vol. 7, no. 12, December-2018.

[23] B. Rim, S. Lee, A. Lee, H.-W. Gil, and M. Hong, "Semantic Cardiac Segmentation in Chest CT Images Using K-Means Clustering and the Mathematical Morphology Method," *Sensors*, vol. 21, no. 8, p. 2675, 2021.

[24] N. Otsu, "A threshold selection method from gray-level histograms," *IEEE Transactions on Systems, Man, and Cybernetics*, vol. 9, no. 1, pp. 62-66, 1979.

[25] M. N. Saad, Z. Muda, N. S. Ashaari, and H. A. Hamid, "Image segmentation for lung region in chest X-ray images using edge detection and morphology," in *2014 IEEE International Conference on Control System, Computing and Engineering (ICCSCE 2014)*, 2014: IEEE, pp. 46-51.

Kuenzang Thinley received the B.Eng. degree in Electronics and Communication Engineering from the College of Science and Technology (CST), Royal University of Bhutan (RUB), Bhutan, in 2019. He is currently pursuing the M.Eng. degree in Electrical Engineering with the Department of Electrical and Computer Engineering, Naresuan University, Phitsanulok, Thailand. He is also an Assistant Lecturer in the Electronics and Communication Department, College of Science and Technology (CST), RUB, Bhutan. His current research interest includes Computer Vision, Image Processing, Signal Processing, and Machine Learning.

Settha Tangkawanit received the B.Eng. degree (Second-class honors) in Computer Engineering, M.Eng. degree in Electrical Engineering and Ph.D degree in Computer Engineering from Naresuan University, in 2005, 2008 and 2019, respectively. Currently, he works at the Department of Electrical and Computer Engineering, Faculty of Engineering, Naresuan University, Phitsanulok, Thailand. His research interests are in the area of embedded system, computer vision, wireless sensor network and Internet of Things.

Surachet Kanprachar received his B.Eng. degree (first-class honors) in Electrical Engineering in 1996 from Chulalongkorn University, Bangkok, Thailand. He received both the M.Sc. and Ph.D. degrees in Electrical Engineering from the Virginia Polytechnic Institute and State University (VA Tech), Blacksburg, Virginia, USA in 1999 and 2003, respectively. Since 2003, he has been with the Department of Electrical and Computer Engineering, Faculty of Engineering, Naresuan University, Phitsanulok, Thailand, where he is now an associate professor. His research interests are in the area of optical fiber communications, coding theory, and artificial intelligence.